Optimal Design of Thermochemical Reactors Based on Constructal Approach

Y. Azoumah, P. Neveu, and N. Mazet
PROMES-CNRS UPR 8521, Laboratoire des Procédés, Matériaux et Énergie Solaire, Tecnosud, Rambla de la Thermodynamique, 66100 Perpignan, France

DOI 10.1002/aic.11152
Published online March 21, 2007 in Wiley InterScience (www.interscience.wiley.com).

This work aims to optimize the design of thermochemical reactors such as solid/gas fixed bed reactors working in dynamic mode. The optimization is based on the constructal approach. A thermodynamic criterion, the ratio of reactor output power to its entropy generation, has to be used to take into account the coupled phenomena and the end purpose of such reactors. Two reactors are considered with same overall volume, but different internal configuration of collectors (constructal scales): a "basic" single-scale configuration (basic reactor), and a "constructal" two-scale configuration (constructal 1 reactor). Reaction rates notably vary with reactor shape, and an optimal shape factor is found for each reactor, depending on the reactant material density. For both reactors, an important remark is pointed out: the correspondence between the maximum of power/entropy ratio (PER) and the highest reaction rate. Comparison between the optimal basic and constructal 1 reactors shows that the latter presents higher energy efficiency (based on second law analysis), but lower output power than the first. © 2007 American Institute of Chemical Engineers *AIChE J,* 53: 1257–1266, 2007
Keywords: optimization, constructal approach, entropy generation, thermochemical reactor, dynamic modeling

Introduction

Several applications involve thermochemical processes such as heat and/or cold production,[1] thermal energy storage,[2] solar deep-freezing,[3] etc. These processes are energy systems in which the main components are as follows:

(1) The thermochemical reactors
(2) The condenser and/or the evaporator

The condenser/evaporator and the thermochemical reactors exchange gas with each other and heat with the environment.[1]

The concept of thermochemical systems is based on thermal effects of a chemical reaction between a gas and a solid carried out by the following equation:

$$\langle S1\rangle + v\mathrm{G} \leftrightarrow \langle S2\rangle + v\Delta H \qquad (1)$$

where
$\langle S1\rangle$: $\langle MX{\cdot}m\mathrm{G}\rangle$ type of reactive solid called discharged salt,
$\langle S2\rangle$: $\langle MX{\cdot}n\mathrm{G}\rangle$ type of reactive solid called charged salt,
v: stoichiometric coefficient ($v = n - m$),
G: gas.

In this solid–gas system, pressure (P) and temperature (T) are linked by Clausis–Clapeyron equation:

$$\ln\left(\frac{P}{P_0}\right) = -\frac{\Delta H}{RT} + \frac{\Delta S}{R} \qquad (2)$$

where P_0 is a reference pressure.

This equation enables to represent solid/gas (S/G) equilibrium conditions and saturation conditions of liquid/gas (L/G) by lines in Clapeyron diagram ($\ln P$, $-1/T$; Figure 1). It is easy to describe the operation of a thermochemical process by this diagram. As shown in Figure 1, the basic cycle of a thermochemical process is composed of two phases:

Correspondence concerning this article should be addressed to Y. Azoumah at this current address: CTEC-Varennes, 1615 Lionel-Boulet, P.O. Box 4800, Varennes, QC, Canada J3X 1S6; e-mail: indusaa@nrcan.gc.ca

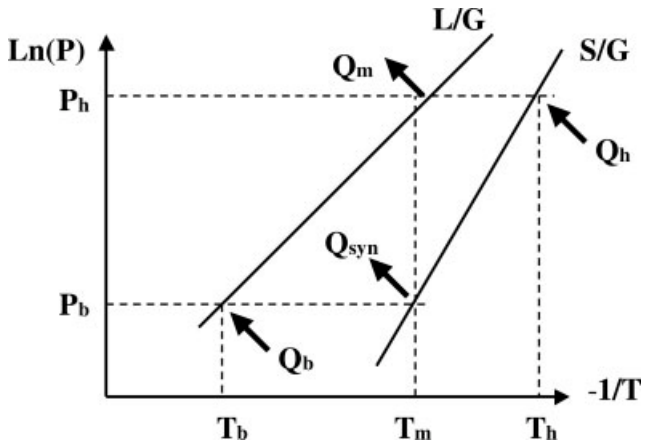

Figure 1. Clapeyron diagram for a thermochemical reactor basic cycle operation.

1. A low pressure phase (P_b) where the synthesis of $\langle S2 \rangle$ is carried out, and heat Q_{syn} is generated at temperature T_m. During this phase, cold Q_b is also produced at the evaporator at temperature T_b.
2. A high pressure phase (P_h) where the solid $\langle S2 \rangle$ is decomposed into ($\langle S1 \rangle + \nu G$). Heat Q_h is supplied at temperature T_h. A gas G is also produced and then condensed at temperature T_m. Heat Q_m is removed at this temperature at the condenser.

The thermochemical reactors, studied in this paper, are filled with a reactive composite material which is composed of expanded natural graphite (ENG),[4] a porous and very compactable matrix, and reactive salts. The permeability and the conductivity of this composite material evolve in antagonistic ways with density.[5] Indeed, ENG conductivity increases when its density does so, whereas at the same time, its permeability decreases. This antagonistic behavior of the permeability and the conductivity has obviously important effects on the reactors performance and design.[6] The challenge is to design, in an optimal way, the architecture of coupled transfer networks—mass and heat—for the thermochemical reactors, in order to improve their power/energy performance.

Our previous articles[7,8] addressed such problems and showed the interest of combining constructal approach and thermodynamic criterion in thermochemical reactors design optimization. The constructal approach developed by Bejan[9] is an interesting tool for the design optimization of engineering systems, such as heat exchangers,[10] fluid distributors,[11] fuel cells,[12] solid–gas reactors,[7,8] and so forth. It is a multiscale geometric method proceeds, which starts from an elemental scale (basic system) to a high scale, constructal system that contains transfer networks. This approach requires an optimization criterion that can be of economic or thermodynamic nature.

We have shown that:[7,8]

(1) entropy generation is a well-adapted optimization criterion for constructal theory when coupled phenomena are taken into account,
(2) for a given reactive material density, (i.e. for given conductivity and permeability), there exists an optimal shape that minimizes the entropy generation of the reactor,
(3) constructing a reactor from elemental scale to upper scales decreases entropy generation, and then should lead to more efficient systems.

For the sake of simplicity, all these investigations were limited to steady state. This paper is devoted to extend these results to instationary systems. In fact, solid/gas thermochemical reactor operates in batch process, in which a charging phase (or synthesis phase) succeeds to a discharging phase (or decomposition phase). During these phases, kinetics evolves, and has to be taken into account as a third irreversible phenomena coupled with heat and mass transfer. Moreover, conductivity and permeability of the reactive material also change with time, as they depend on the reaction conversion.

Beside these changes, which only concern the modeling work, optimization criterion has also been redefined: entropy generation minimization attracts the reactive system near equilibrium conditions, and then leads to zero output power systems! A new criterion emerges from preliminary work, expressed as temperature (in Kelvin) and defined as the ratio between output power and entropy generation. Only a basic reactor and a constructal 1 reactor are considered for this study. A basic reactor is a reactor with constructal scale "zero," whereas a constructal 1 reactor (assembly of optimal elemental volumes) is a tree-network reactor at the first constructal scale as defined in our previous work.[8]

Dynamic Modeling

Figures 2a,b represent, respectively, the cross section of the basic reactor and of the constructal 1 reactor. These reactors are parallelepiped. For the sake of simplicity, heat collector and gas diffuser are assumed to be combined in a single element named "integrated collector" as described in our previous work.[8] Integrated collectors are tagged in red in Figures 2a,b. The remaining part of the reactors is filled with the reactive composite material in which a chemical reaction occurs, consuming gas and generating heat. As a consequence, the heat source and the gas sink are linked by the reaction enthalpy ΔH (Eqs. 5 and 6). The heat (the gas) is collected through the integrated collectors to (from) the reactor boundary.

The shape factor (f) of a reactor is defined as the ratio of its dimensions (H and L); $f = H/L$. For instance, the shape factor of the basic reactor is $f_0 = H_0/L_0$, and the shape factor of the constructal 1 reactor is $f_1 = H_1/L_1$ (Figures 2a,b). These shape factors are not fixed, but the reactor thickness (W) and its area ($A = HL$) are fixed, so is the reactor volume ($V = AW$). The shape factor will be the optimization variable for this investigation.

Modeling of the reactor

For the two reactors, we have

- In the integrated collectors, heat and mass balances are

$$\rho_p c \frac{\partial T}{\partial t} = \mathrm{div}(\lambda_p \mathrm{grad} T) \tag{3}$$

$$\frac{\xi_p}{RT} \frac{\partial P}{\partial t} = \mathrm{div}\left[\left(\frac{k_p P}{\mu RT}\right)\mathrm{grad} P\right] \tag{4}$$

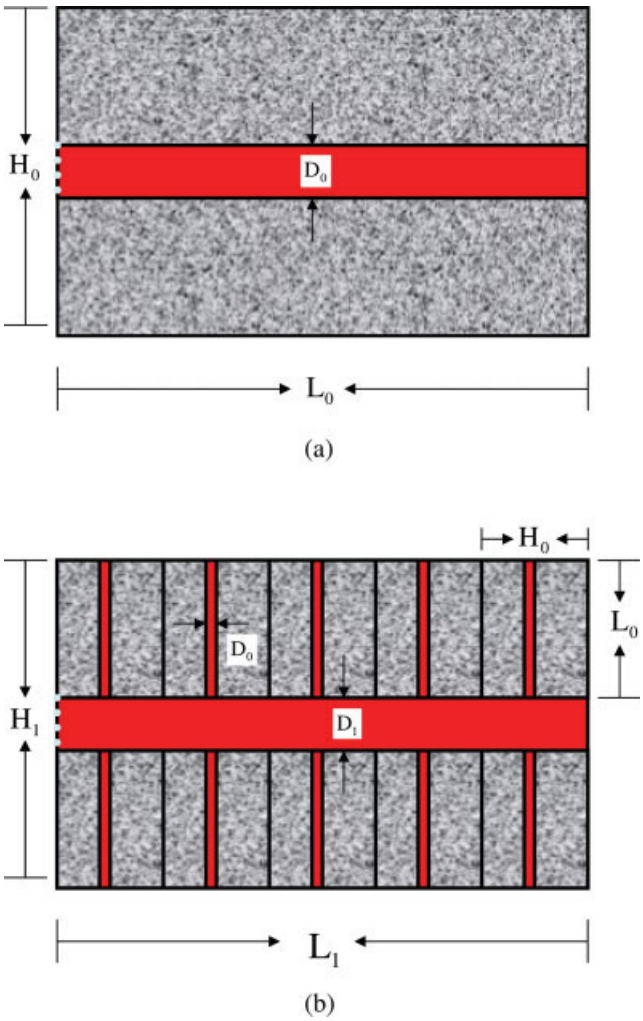

Figure 2. a: Basic reactor; b: Constructal 1 reactor.

[Color figure can be viewed in the online issue, which is available at www.interscience.wiley.com.]

• In the reactive composite material, heat and mass balances and the chemical kinetics are respectively expressed by

$$\rho_0 C_0 \frac{\partial T}{\partial t} = \mathrm{div}(\lambda_0 \mathrm{grad} T) + vN\Delta H \frac{dX}{dt} \tag{5}$$

$$\frac{\xi_0}{RT}\frac{\partial P}{\partial t} = \mathrm{div}\left[\left(\frac{k_0 P}{\mu RT}\right)\mathrm{grad} P\right] - vN\frac{dX}{dt} \tag{6}$$

$$\frac{dX}{dt} = \mathrm{Arh}(1-X)\left(1-\frac{P_{\mathrm{eq}}}{P}\right) \tag{7}$$

In Eq. 5, X is the reaction conversion while $\rho_0 C_0$ is the thermal capacity of the reactive composite material and can be expressed as

$$\rho_0 C_0 = \frac{m_{\mathrm{graphite}} C_{\mathrm{graphite}}}{V_0} + \frac{N}{V_0}\left(\bar{C}_{\mathrm{salt}} + vX\bar{C}_{\mathrm{gas}}\right) \tag{8}$$

In Eq. 7, Arh is defined as Arrhenius constant and P_{eq} is the thermodynamic equilibrium pressure which is expressed as

$$P_{\mathrm{eq}} = \exp\left(-\frac{\Delta H}{RT} + \frac{\Delta S}{R}\right) \tag{9}$$

The local entropy generation, deduced from the first and the second laws of thermodynamics, and Gibbs equation[13] is expressed, respectively, for the integrated collector and the composite material as

$$\dot{\sigma}_{\mathrm{col}} = \frac{\lambda_{\mathrm{p}}}{T^2}(\mathrm{grad}T)^2 + \frac{k_{\mathrm{p}}}{\mu \mathrm{T}}(\mathrm{grad}P)^2 \tag{10}$$

$$\dot{\sigma}_{\mathrm{mat}} = \frac{\lambda_0}{T^2}(\mathrm{grad}T)^2 + \frac{k_0}{\mu T}(\mathrm{grad}P)^2 + vNR\ \ln\left(\frac{P}{P_{\mathrm{eq}}}\right)dX/dt \tag{11}$$

These two expressions clearly show the contribution of each process, namely the heat and mass transfer, and the chemical kinetics.

N: molar density of the reactive solid (mol m^{-3}).

dX/dt is the reaction rate (s^{-1}) and $R\ \ln(P/P_{\mathrm{eq}})$ is the affinity of the reaction.

Initial and boundary conditions

Initially, the reactors are assumed to be at the equilibrium temperature T_{eq} (so in equilibrium pressure P_{eq}), except for the left-hand part of the integrated collector (Figures 2a,b), tagged by green dots, where the constraint temperature T_{c} and the constraint pressure P_{c} are imposed. Furthermore, the walls of the reactors are assumed adiabatic and impermeable, except the left end of the integrated collector where the temperature T_{c} and pressure P_{c} are fixed.

Transfer properties modeling

The reactive material conductivity and permeability are linked to its density which is itself a function of the chemical reaction conversion[5]: chemical reaction implies not only an enthalpy change (thermal effect) but also a volume change. As the synthesis phase progresses, reactive material density decreases. Adding a certain amount of ENG permits to "absorb" this volume change, but the porosity of the mixture evolve accordingly during the reaction.

This effect has been extensively studied in the last decade,[5,14] and results showed some correlations reported in Appendix. These correlations permit to compute both conductivity and permeability as functions of reaction conversion X.

Thermodynamic Optimization Criterion and Numerical Simulation Procedure

In our previous works,[7,8] the power generated by the reactors was fixed, because the chemical kinetics was assumed constant. Unlike these previous works, here the generated power inside the reactor ($\dot{Q}_{\mathrm{gen}}$) is a function of the reaction rate dX/dt and the enthalpy of the reaction ΔH.

$$\dot{Q}_{\mathrm{gen}} = \Delta H \frac{dX}{dt} \tag{12}$$

Table 1. Integrated Collectors Characteristics

Collector fraction, ε_0	0.01
Collector porosity, ξ_p	0.9
Collector density, ρ_p	2702 kg m^{-3}
Thermal capacity of the collector, c	903 J kg^{-1} K^{-1}
Thermal conductivity of the collector, λ_p	237 W m^{-1} K^{-1}
Permeability of the collector, k_p	10^{-10} m^2

However, the user is interested in the output power of the reactor ($\dot{Q}_S$). Because of dynamics, this power is different from the one generated inside the reactor at a given time t. Its expression is

$$\dot{Q}_S = \iint_S J_s \, ds \tag{13}$$

where J_s is the heat flux density extracted from the integrated collector, and s is the collector area.

This output power varies in the course of the time t; it is then necessary to take into account this power variation in the optimization criterion. Furthermore, a system with a great power and almost reversible (low entropy generation) is more interesting than a system that produces low entropy generation and which has a weak power (or a system with a great power and which generates much entropy). As a consequence, a new optimization criterion is chosen here: the reactor output power over its entropy generation, which is defined by "power/entropy ratio" (PER) in this paper. The maximization of the PER is achieved with respect to the reactor shape factor. In the following sections, the power/entropy ratio is referred to as PER.

Numerical simulation procedure

The simulation of a reactor consists in determining its cross-section temperature (T) and pressure (P) fields as well as the reaction conversion (X). Local entropy productions of integrated collectors and of composite reactive material are then evaluated. The total entropy generation of each domain (integrated collectors, remaining part of the reactor) is obtained by integration over time and space. The reactor output power is also evaluated by integration over time and space over the external boundary of the integrated collector (see Eq. 13).

Optimization is carried out by finding the shape factor maximizing the PER. This is done using Femlab®[15] and Matlab®.[16] Femlab is a graphical interface where the reactor geometry is defined, along with associated equations and initial and boundary conditions. The space integration is based on finite elements.[17] The mesh grid of the reactor is automatically generated at the level of the graphical interface. Femlab temporal solvers offer all the time step calculations automatically. The solver chosen for this simulation is called FLDASPK; it is quick and well-adapted to this study.

Table 2. Gas and Reactive Material Characteristics

Reactive material porosity, ξ_0	0.6
ENG apparent density, $\tilde{\rho}_0$	50–120 kg m^{-3}
Molar mass of the salt, M_{salt}	160 g mol^{-1}
Molar mass of the gas, M_{gas}	17 g mol^{-1}
Salt mass ratio, W_s	0.75
Thermal capacity of the gas, C_{gas}	80.27 J mol^{-1} K^{-1}
Thermal capacity of the salt, C_{salt}	72.26 J mol^{-1} K^{-1}
Thermal capacity of ENG, $C_{graphite}$	733.15 J kg^{-1} K^{-1}
Enthalpy of the reaction, ΔH	47,416 J mol^{-1}
Entropy of the reaction, ΔS	228.07 J K^{-1}
Arrhenius constant, Arh	0.003 s^{-1}
Area of the reactors, A_0	0.05 m^2

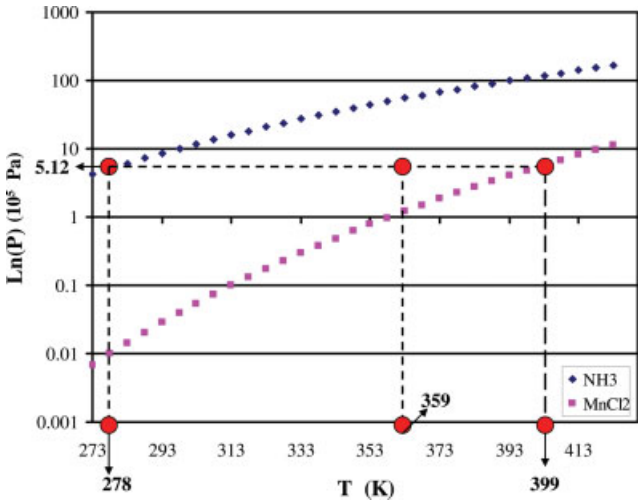

Figure 3. Thermodynamic equilibrium conditions for NH_3 liquid/gas and $MnCl_2$ (6/2)/NH_3.

[Color figure can be viewed in the online issue, which is available at www.interscience.wiley.com.]

Simulation parameters

The solid–gas pair chosen for simulations is $MnCl_2/NH_3$ that reacts according to:

$$\langle MnCl_2, 2NH_3\rangle + 4(NH_3) \leftrightarrows \langle MnCl_2, 6NH_3\rangle + \Delta H \tag{14}$$

Only the synthesis phase is considered in this study.

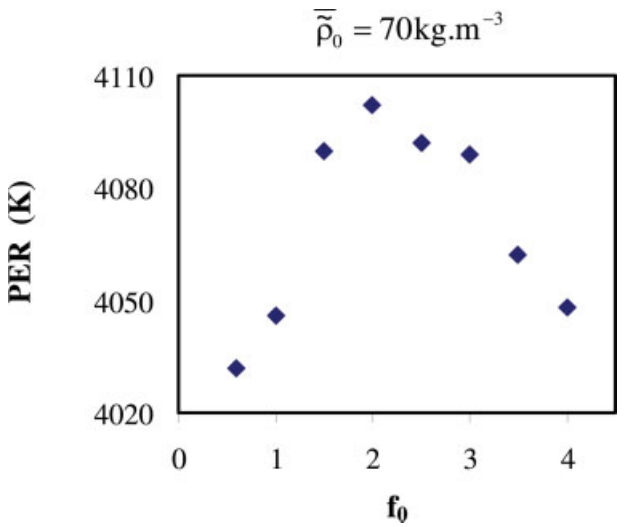

Figure 4. PER vs. reactor shape factors of the basic reactor for $\tilde{\rho}_0$ = 70 kg m^{-3}.

[Color figure can be viewed in the online issue, which is available at www.interscience.wiley.com.]

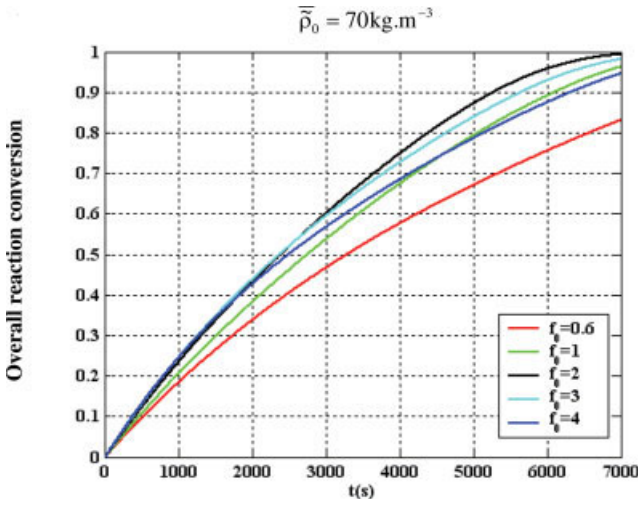

Figure 5. Overall reaction conversion of different reactor shape factors vs. time (t) for $\bar{\bar{\rho}}_0 = 70$ kg m^{-3}.

[Color figure can be viewed in the online issue, which is available at www.interscience.wiley.com.]

Tables 1 and 2 contain all the simulation parameters for the integrated collectors, and the reactive material and gas, respectively.

Figure 3 shows the operating conditions used for the numerical simulation. A temperature $T_{ev} = 278$ K is imposed at the evaporator; the corresponding liquid/gas equilibrium pressure is $P_{eq}(T_{ev}) = 5.12 \times 10^5$ Pa. For the solid/gas equilibrium, the corresponding temperature is $T_{eq} = 399$ K, as shown in Figure 3. For the synthesis phase to start, one must impose a reactor temperature drop ($T_c - T_{eq}$), where T_c is a constraint temperature and T_{eq} is an equilibrium temperature. Here, $T_c = 359$ K is imposed, and the constraint pressure is $P_c = 5.12 \times 10^5$ Pa.

Results and Discussion

Simulation is done for several reactive composite materials with different apparent densities (Table 2) often used in our reactors. These apparent densities lead to conductivities in the range of 1.7–27 W m^{-1} K^{-1} and mean permeabilities in the range of $8 \times 10^{-9} - 2 \times 10^{-13}$ m^2.

The basic reactor

Figure 4 shows the variation of the PER vs. the shape factor for ENG apparent density, $\bar{\bar{\rho}}_0 = 70$ kg m^{-3}. The PER does not vary much with the factor shapes. However, the optimal shape factor is $f_0 = 2$ because it has the maximum PER. In Figure 5, one can see that the corresponding reaction

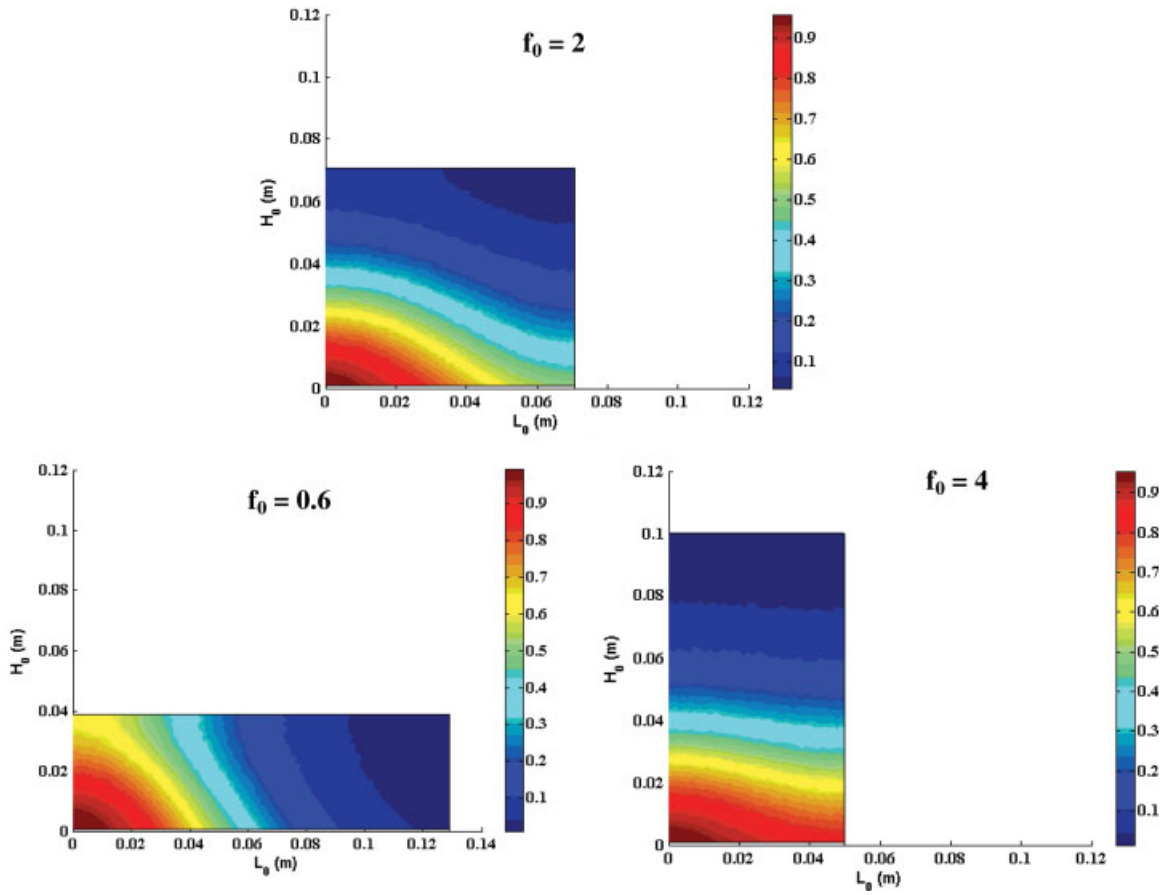

Figure 6. Local reaction conversion field for shape factors $f_0 = 2$, $f_0 = 0.6$, and $f_0 = 4$ at overall conversion $X_g = 0.3$.

[Color figure can be viewed in the online issue, which is available at www.interscience.wiley.com.]

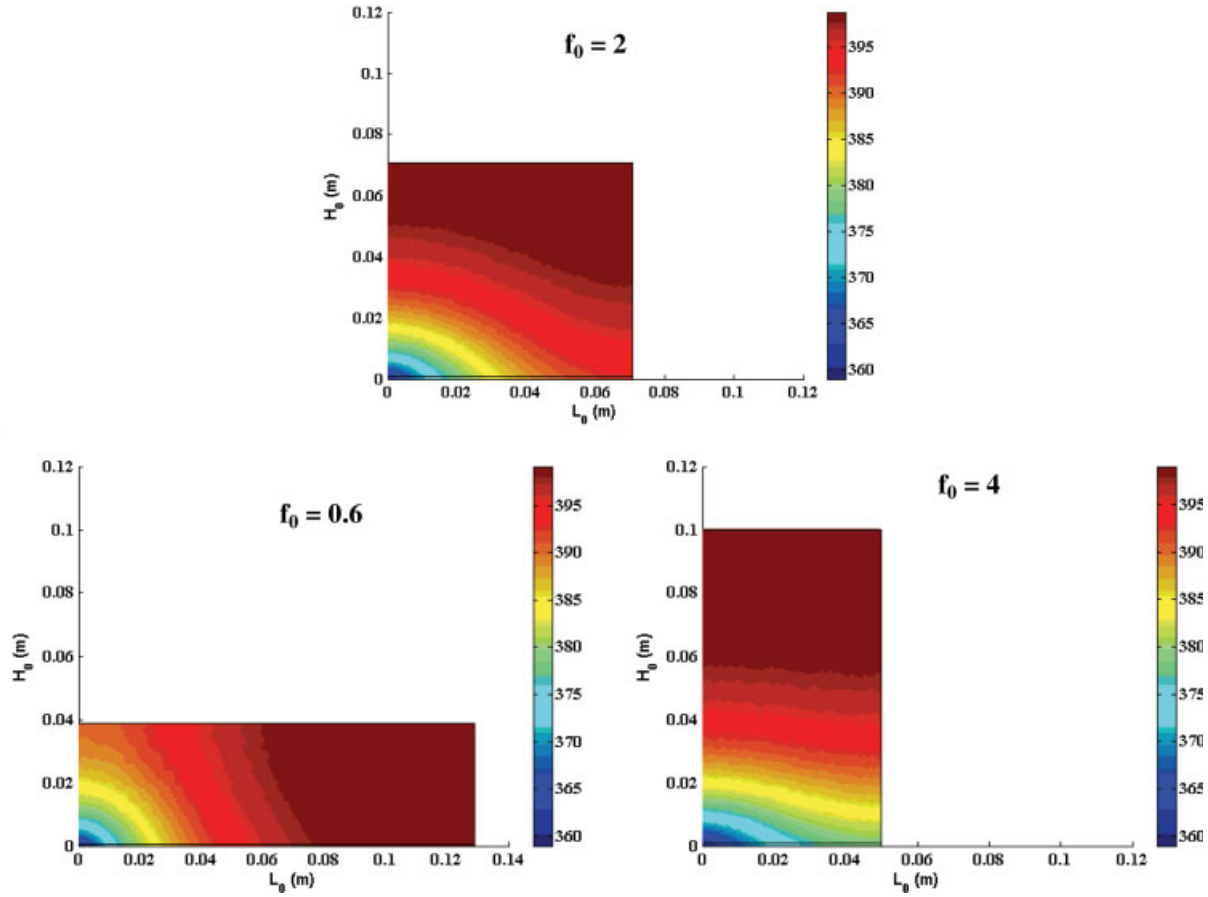

Figure 7. Local temperature field for shape factors f_0 = 2, f_0 = 0.6, and f_0 = 4 at overall conversion X_g = 0.3.

[Color figure can be viewed in the online issue, which is available at www.interscience.wiley.com.]

rates vary considerably with the shape factor. Moreover, a correspondence is observed between the greatest reaction rate and the maximum of PER. This result is very interesting, because it is not obvious a priori and could help in practice: for instance, the knowledge of the reactor reaction rates could automatically help in having an idea on their thermodynamic efficiency without other evaluations.

Figures 6 and 7 respectively, display the reaction conversion field and the temperature field, at the overall conversion $X_g = 0.3$, for three shape factors: $f_0 = 0.4$, $f_{0,opt} = 2$ (optimal shape factor) and $f_0 = 4$. Because of symmetry, only half of the reactors are plotted here. We note first that the inactive zones (blue zones where chemical reaction does not occur yet) on Figure 6 correspond to the zones where we have almost the equilibrium temperature $T_{eq} = 399$ K on Figure 7 (red zones). This is often observed experimentally. We also note that inactive zones are more important for the shape factors $f_0 = 0.2$ and $f_0 = 4$ than for the optimal shape factor $f_{0,opt} = 2$. This important result matches with the fact that the reaction is quicker in the optimal shape reactor than in nonoptimal ones (Figure 5).

Figures 8–10 show the PER vs. the shape factors for various ENG apparent densities: $\bar{\tilde{\rho}}_0 = 50$ kg m^{-3}, $\bar{\tilde{\rho}}_0 = 80$ kg m^{-3}, and $\bar{\tilde{\rho}}_0 = 120$ kg m^{-3}. For each ENG apparent density, there exits an optimal shape factor for the reactor: $f_{0,opt} = 2$ for $\bar{\tilde{\rho}}_0 = 50$ kg m^{-3} and $\bar{\tilde{\rho}}_0 = 80$ kg m^{-3}, and $f_{0,opt} = 3$ for $\bar{\tilde{\rho}}_0 = 120$ kg m^{-3}. An analogous behavior was reported in our previous work,[8] limited to steady state, in which the optimization criterion was the minimization of the reactor entropy generation.

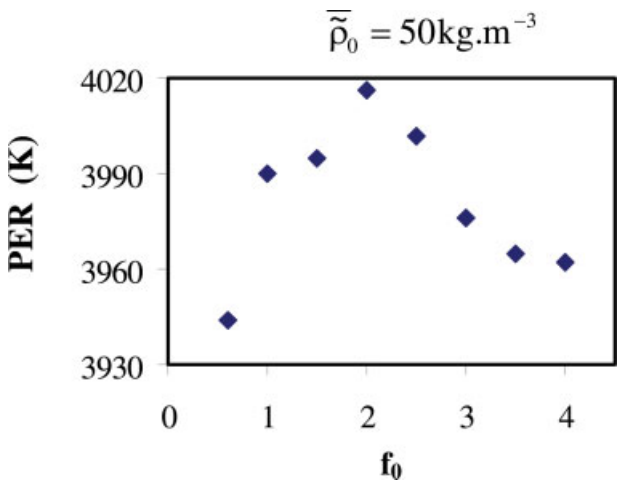

Figure 8. PER vs. reactor shape factors for $\bar{\tilde{\rho}}_0$ = 50 kg m^{-3}.

[Color figure can be viewed in the online issue, which is available at www.interscience.wiley.com.]

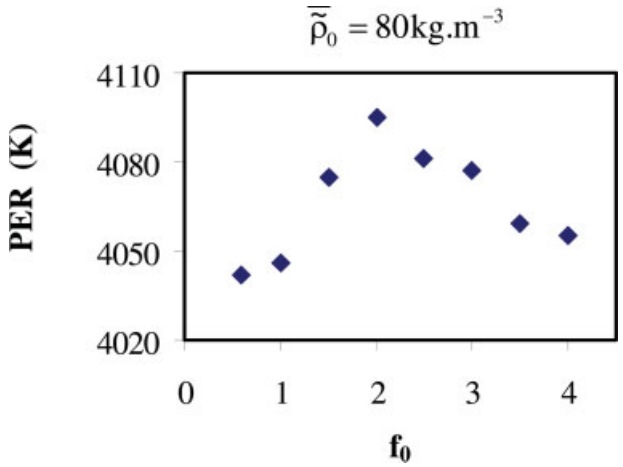

Figure 9. PER vs. reactor shape factors for $\bar{\tilde{\rho}}_0$ = 80 kg m^{-3}.

[Color figure can be viewed in the online issue, which is available at www.interscience.wiley.com.]

Figures 11–13 respectively, show the overall reaction conversion corresponding to $\bar{\tilde{\rho}}_0$= 50 kg m^{-3}, $\bar{\tilde{\rho}}_0$ = 80 kg m^{-3}, and $\bar{\tilde{\rho}}_0$ = 120 kg m^{-3}. Reaction rates vary with the shape factor for the apparent densities selected. Furthermore, the correspondence between the maximum of PER and the highest reaction rate is also observed here for all apparent densities.

Optimal shape factors of the reactor increase with the ENG apparent density as shown in Figure 14. In other words, optimal reactor shapes become more and more slender when the ENG apparent density increases.

Constructal 1 reactor

Numerical simulation results of the constructal 1 reactor are presented in this part. Recall that this reactor has the same optimization constraints as the basic reactor: same volume V_0 and same composition of the reactive composite material (ENG + salt). The simulation parameters are identical as for the basic reactor (Tables 1 and 2).

Constructal 1 reactor consists of an assembly of n_1 optimal elemental volumes. These optimal elemental volumes have the same shape factor as the basic reactor, but a lower volume v_0 such as $n_1 v_0 + v_{col} = V_0$ (v_{col} is here the collectors volume) according to the optimization constraints recalled earlier. Their number n_1 is deduced from the optimal shape f_1 of the constructal 1 reactor and of the optimal elemental volume f_0 through the following relation[8]: $n_1 = 4/f_1 f_0 (1 - \varepsilon_1)$. In this relation, $\varepsilon_1 = A_{1p}/A_1 = D_1/H_1$ is the ratio of the integrated collector area to the constructal 1 reactor area (Figure 2b), named "collector fraction" in this article.

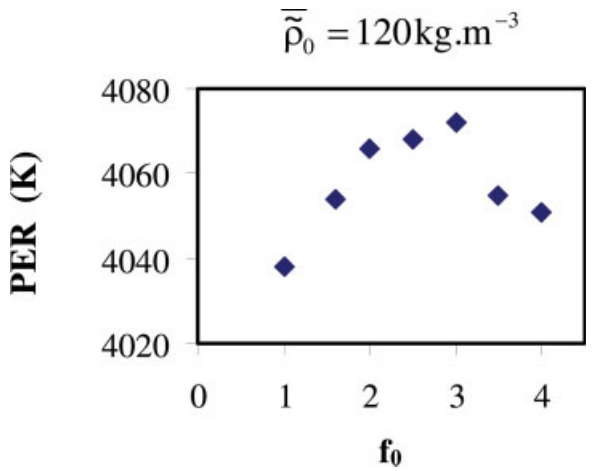

Figure 10. PER vs. reactor shape factors for $\bar{\tilde{\rho}}_0$ = 120 kg m^{-3}.

[Color figure can be viewed in the online issue, which is available at www.interscience.wiley.com.]

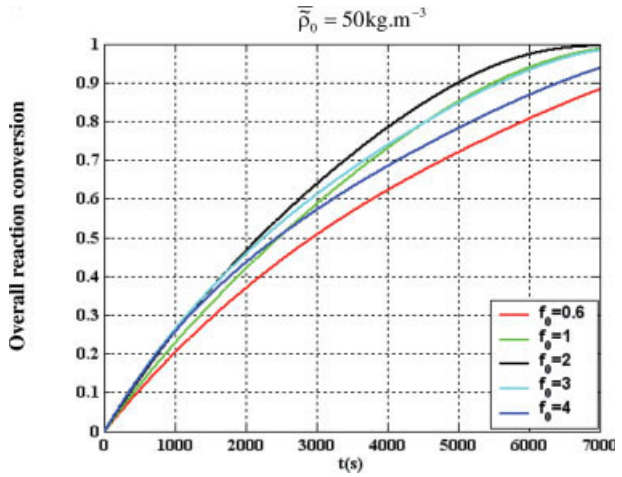

Figure 11. Overall reaction conversion of different reactor shape factors vs. time (t) for $\bar{\tilde{\rho}}_0$ = 50 kg m^{-3} ($f_{0,opt}$ = 2).

[Color figure can be viewed in the online issue, which is available at www.interscience.wiley.com.]

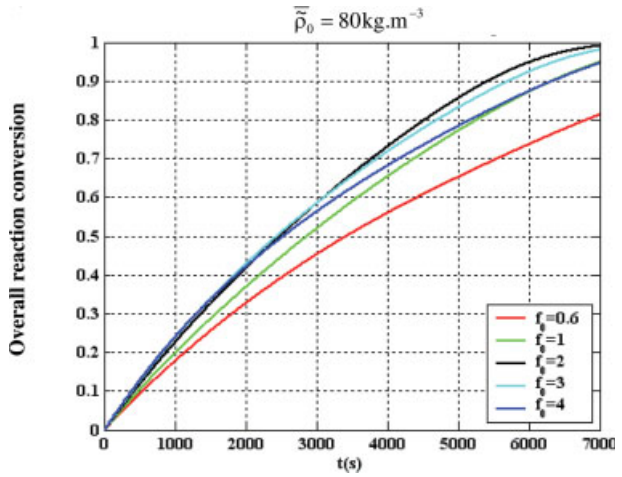

Figure 12. Overall reaction conversion of different reactor shape factors vs. time (t) for $\bar{\tilde{\rho}}_0$ = 80 kg m^{-3} ($f_{0,opt}$ = 2).

[Color figure can be viewed in the online issue, which is available at www.interscience.wiley.com.]

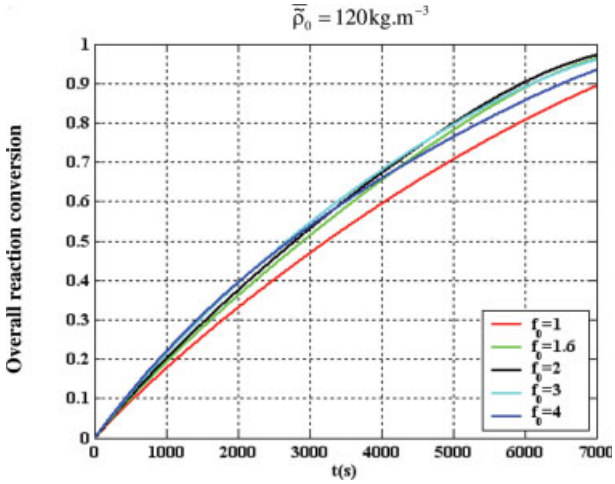

Figure 13. Overall reaction conversion of different reactor shape factors vs. time (t) for $\overline{\tilde{\rho}}_0$ = 120 kg m^{-3} ($f_{0,opt}$ = 3).

[Color figure can be viewed in the online issue, which is available at www.interscience.wiley.com.]

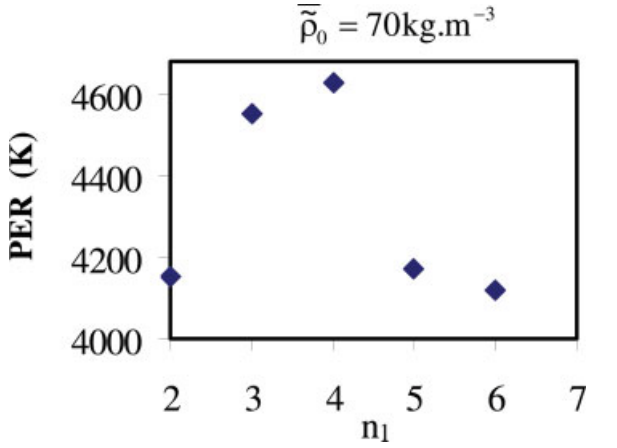

Figure 15. PER vs. elemental volumes numbers for $\overline{\tilde{\rho}}_0$ = 70 kg m^{-3}.

[Color figure can be viewed in the online issue, which is available at www.interscience.wiley.com.]

Figure 15 shows the PER vs. elemental volume number n_1 that compose the constructal 1 reactor. An optimal number ($n_{1,opt}$ = 3), and so an optimal shape factor, exists for the ENG apparent density selected, $\overline{\tilde{\rho}}_0$ = 70 kg m^{-3}. The corresponding overall reaction conversions, plotted in Figure 16, considerably vary with the elemental volume number. Here, the correspondence between the maximum PER and the greatest reaction rate is also pointed out.

Comparison of the optimal basic reactor and the optimal constructal 1 reactor for $\overline{\tilde{\rho}}_0$ = 70 kg m^{-3}

Figure 17 shows that the reaction rate of the optimal basic reactor is greater than that of the optimal constructal 1 reactor. In other words, the optimal basic reactor is more powerful than the optimal constructal 1 reactor. However, the corresponding PER for the optimal constructal 1 reactor (4420 K) is greater than that of the optimal basic reactor (3621 K). Likewise, if we fix the overall reaction conversion at X = 0.8 for the two optimal reactors (Figure 17); the constructal 1 reactor has a greater PER (4420 K) than the basic reactor (3561 K). This result shows that the basic reactor, despite the fact that it is the most powerful, produces much more entropy than the optimal constructal 1 reactor. The conclusion here is that, from an energy effectiveness point of view, based on a second law analysis, the optimal constructal 1 reactor is preferable to the optimal basic reactor for the ENG apparent density selected.

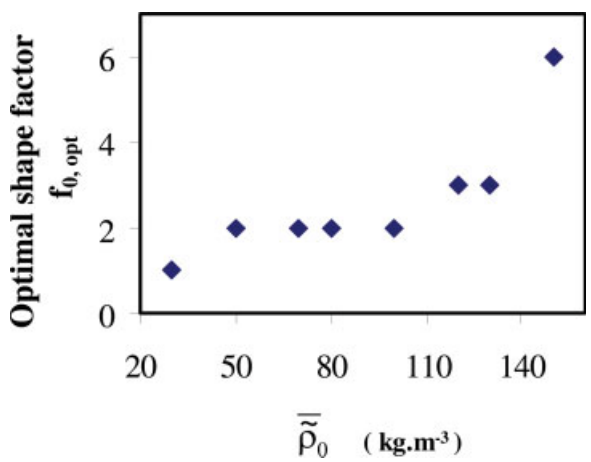

Figure 14. Evolution of optimal shape factors with the ENG apparent density.

[Color figure can be viewed in the online issue, which is available at www.interscience.wiley.com.]

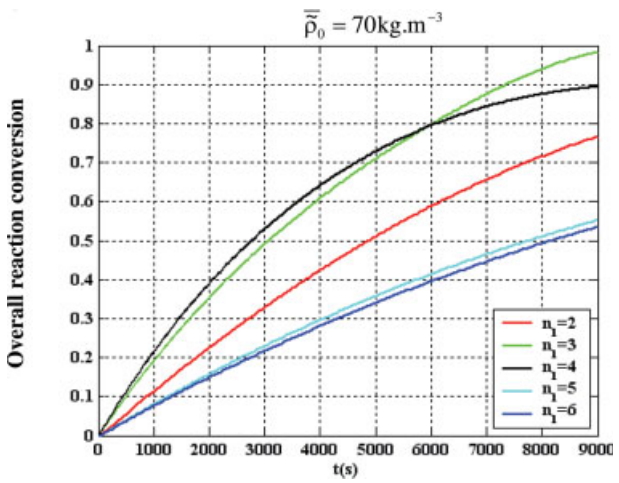

Figure 16. Overall reaction conversion of different elemental volumes numbers vs. time (t) for $\overline{\tilde{\rho}}_0$ = 70 kg m^{-3} ($n_{1,opt}$ = 3).

[Color figure can be viewed in the online issue, which is available at www.interscience.wiley.com.]

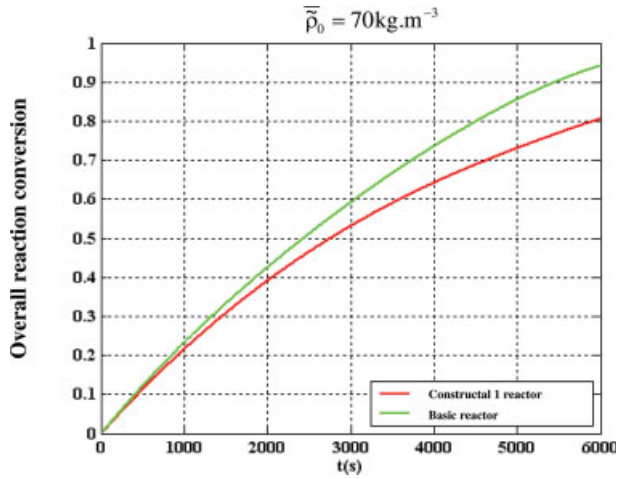

Figure 17. Overall reaction conversion of optimal basic reactor and optimal constructal 1 reactor vs. time (t) for $\bar{\tilde{\rho}}_0 = 70$ kg m^{-3}.

[Color figure can be viewed in the online issue, which is available at www.interscience.wiley.com.]

Conclusion

This article deals with the dynamic optimization of thermochemical reactors. Two reactors were considered for the numerical simulation: a basic reactor and a constructal 1 reactor. A new thermodynamic optimization criterion is considered in this study: the maximization of the output power of the reactor to its entropy generation ratio, because the output power varies in the course of the time.

For the basic reactor, we show that there exists an optimal shape factor, regardless of the density of the composite material. Our previous work,[7] limited to steady state, showed the same result. An interesting correspondence is also pointed out between the maximum PER and the greatest reaction rate for a given ENG apparent density.

For the constructal 1 reactor, an optimal number of the elemental volumes ($n_{1,\text{opt}} = 3$) is found for the ENG apparent density selected. As for the basic reactor, the maximum PER also corresponds to the greatest reaction rate.

Finally, we compare the optimal basic reactor and the optimal constructal 1 reactor for the same ENG apparent density. This comparison shows that the optimal basic reactor is more powerful than the constructal 1 reactor, but the latter has a better second law energy performance than the first.

Acknowledgments

Financial support from French Ministry of Research and Technology is gratefully acknowledged.

Notation

A_i = area of reactors, m^2
C = thermal capacity of the collector, J kg^{-1} K^{-1}
$\bar{C}_{\text{gas}}$ = molar thermal capacity of the gas, J mol^{-1} K^{-1}
C_{graphite} = thermal capacity of ENG, J kg^{-1} K^{-1}
$\bar{C}_{\text{salt}}$ = molar thermal capacity of the salt, J mol^{-1} K^{-1}
f_i = shape of constructal i reactor, $f_i = H_i/L_i$
H_i = height of constructal i reactor, m
k_i = permeability of constructal i reactor material, m^2
k_p = permeability of the collector, m^2
L_i = length of constructal i reactor, m
n_1 = number of elemental volumes assembled in the constructal 1 reactor
P = pressure, Pa
PER = power/entropy ratio K
R = ideal gas constant, J mol^{-1} K^{-1}
t = time, s
T = temperature, K
V_0 = volume of the reactors, m^3
W = thickness of the reactors, m

Greek letters

ΔH = enthalpy of reaction, J mol^{-1}
ΔS = entropy of the reaction, J mol^{-1} K^{-1}
ε_0 = collector fraction
ξ_p = collector porosity
ξ_0 = reactive material porosity
λ_i = thermal conductivity of the reactive material at the scale i, W m^{-1} K^{-1}
λ_p = thermal conductivity of collectors, W m^{-1} K^{-1}
μ = gas dynamic viscosity, kg m^{-1} s^{-1}
ν = stoichiometric coefficient
ρ_p = collector density, kg m^{-3}
ρ_0 = density of the reactive material, kg m^{-3}
$\tilde{\rho}_0$ = ENG apparent density, kg m^{-3}

Subscripts

opt = optimum
i = constructal scale

Literature Cited

1. Goetz V, Spinner B, Lepinasse E. A solid–gas thermochemical cooling system using $BaCl_2$ and $NiCl_2$. *Energy*. 1996;22:49–58.
2. Lahmidi H, Mauran S, Goetz V. Definition, test and simulation of a thermochemical storage process adapted to solar thermal systems. *Solar Energy*. 2006;80:883–893.
3. Le Pierrès N, Stitou D, Mazet N. New deep-freezing process using renewable low-grade heat: from the conceptual design to experimental results. *Energy*. 2007;32:600–608.
4. Coste C, Crozat G, Mauran S. US patent 4,595,774. 1986.
5. Olives R, Mauran S. A highly conductive porous medium for solid-gas reactions: effect of the dispersed phase on the thermal tortuosity. *Transport Porous Media*. 2001;43:377–394.
6. Jolly P, Mazet N. Optimisation de la diffusion du gaz dans les matériaux réactifs, siège de transferts de chaleur, de masse et d'une réaction chimique. *Int J Heat Mass Transfer*. 1999;42:303–321.
7. Azoumah Y, Mazet N, Neveu P. Constructal network for heat and mass transfer in a solid–gas reactive porous medium. *Int J Heat Mass Transfer*. 2004;47:2961–2970.
8. Azoumah Y, Neveu P, Mazet N. Constructal design combined with entropy generation minimization for solid–gas reactors. *Int J Therm Sci*. 2006;45:716–728.
9. Bejan A. Shape and Structure, from Engineering to Nature. Cambridge: Cambridge University Press, 2000.
10. Bonjour J, Rocha LAO, Bejan A, Meunier F. Dentritic fins optimization for a coaxial two-stream heat exchanger. *Int J Heat Mass Transfer*. 2003;47:111–124.
11. Tondeur D, Luo L. Design and scaling laws of ramified fluid distributors by the constructal approach. *Chem Eng Sci*. 2004;59:1799–1813.
12. Vargas JVC, Ordonez JC, Bejan A. Constructal flow structure for a PEM fuel cell. *Int J Heat Mass Transfer*. 2004;47:4257–4263.
13. Prigogine I, Kondepudi D. Modern Thermodynamics: From Heat Engines to Dissipative Structures. New York: Wiley, 1998.
14. Mauran S. Flux de gaz en milieu poreux réactif déformable: relation entre texture, propriétés mécaniques et transferts. Incidence sur la mise en œuvre des réactifs et les performances de pompes à chaleur chimiques solide–gaz. Ph.D. Thesis, Universty of Perpignan, 1990.

15. Femlab User's Guide and Introduction (Version 2.3). Stockholm: COMSOLAB, 2003.
16. Borse GJ. Numerical Methods with Matlab. Boston: PWS Publishing Company, 1997.
17. Chuang TJ. Finite Elements Analysis in Fluid Dynamics. New York: MacGraw Hill, 1978.

Appendix

Conductivity modeling

Olivès and Mauran[5] established an empirical relation that enables to express the conductivity λ_0 as follows:

$$\lambda_0 = \lambda_\perp (1 + \alpha f_s)^{-2} \tag{A1}$$

where

$$\lambda_\perp = \lambda_* (\bar{\tilde{\rho}}_0 / \tilde{\rho}_*)^{(4/3+0.17)} \tag{A2}$$

where

$\lambda_* = 3.70$ W m^{-1} K^{-1},

$\bar{\tilde{\rho}}_0$: apparent density of ENG (kg m^{-3}),

α: coefficient identified for the reactive composite material; its value equals 1.2 in this study,

f_s is the volume fraction of the salt which is expressed by

$$f_s \left(\frac{\bar{\tilde{\rho}}_0}{\rho_s (1 - \varepsilon_g)} \right) \left(\frac{w_s}{1 - w_s} \right) \tag{A3}$$

where

ρ_s salt density (kg m^{-3}),

ε_g porosity of the salt grains,

$w_s = m_{salt}/(m_{salt} + m_{graphite})$ is the mass percentage of the salt contained in the reactive composite material (named as "salt mass ratio" in this article).

Permeability modeling

Mauran[14] has studied the permeability evolution of the composite material, with respect to the manufacturing parameters. He established an empirical correlation that expresses the material permeability k_0 as function of an overall parameter $\tilde{\rho}_{leX}$. It yields

$$\log(k_0) = -4 - 4.3 \ \log(\tilde{\rho}_{leX}) \tag{A4}$$

where $\tilde{\rho}_{leX}$ is defined as follows:

$$\tilde{\rho}_{leX} = \frac{\text{ENG mass}}{\text{reactor volume} - \text{volume occupied by salt grains}} \tag{A5}$$

$$\tilde{\rho}_{leX} = \frac{m_b}{\tilde{V}_m - \tilde{V}_{sX}} = \left[\frac{1}{\bar{\tilde{\rho}}_0} - \frac{w_s}{(1 - w_s)} \ \frac{v_{sX}}{M_{sa}(1 - \varepsilon_g)} \right]^{-1} \tag{A6}$$

In the expression (A6) $\tilde{V}_m$ is the apparent volume of the reactive composite material, whereas $\tilde{V}_{sX}$ is the apparent volume occupied by salt grains at a given reaction conversion rate X.

ε_g is the intern porosity of the salt grains, and its value is considered here to be 0.3.

V_{sX} is the effective volume occupied by salt grains at a given reaction conversion rate X; its expression is

$$V_{sX} = (1 - X) V_{s0} + X V_{sl} \tag{A7}$$

V_{s0} and V_{s1} are, respectively, the molar volumes of the charged salt and the uncharged salt.

Manuscript received May 12, 2005, and revision received Feb. 16, 2007.